NAGW-1118

Relationships of Soil, Grass, and Bedrock over the Kaweah Serpentinite Melange Through Spectral Mixture Analysis of AVIRIS Data

John F. Mustard
Department of Geological Sciences
Brown University
Providence RI 02912
(401) 863-1264

submitted to:

Remote Sensing of Environment
December 1991

This manuscript is printed and copied on recycled paper (50% Post-industrial and 10% post-consumer waste)

Abstract

A linear mixing model is used to model the spectral variability of an AVIRIS scene from the western foothills of the Sierra Nevada and calibrate these radiance data to reflectance. Five spectral endmembers from the AVIRIS data, plus an ideal "shade" endmember were required to model the continuum reflectance of each pixel in the image. Three of the endmembers were interpreted to model the surface constituents green vegetation, dry grass, and illumination. These are the main transient surface constituents that are expected to change with shifts in land use or climatic influences and viewing conditions ("shade" only). The spectral distinction between the other three endmembers is very small, yet the spatial distributions are coherent and interpretable. These distributions cross anthropogenic and vegetation boundaries and are best interpreted as different soil types. Comparison of the fraction images to the bedrock geology maps indicates that substrate composition must be a factor contributing to the spectral properties of these endmembers. Detailed examination of the reflectance spectra of the three soil endmembers reveals that differences in the amount of ferric and ferrous iron and/or organic constituents in the soils is largely responsible for the differences in spectral properties of these endmembers.

I Introduction

As Earth Science evolves into the era of the Earth Observing System, with increasing emphasis being placed on issues related to global change (Committee on Earth Sciences, 1990), it is becoming ever more important to apply quantitative modelling techniques to remote sensing data. Remote sensing will play a vital role in global change research because of the synoptic coverage of land surfaces, repeat measurements through time, and the numeric-, and therefore quantitative-nature of the data. For land surfaces, modelling approaches are needed that characterize the primary surface constituents quantitatively and are based on a realistic and reproducible description of the surface. This is required for the identification of the precise amount of change occurring in transient surface constituents that respond rapidly to changes in land use or climate relative, to surface constituents that do not change or change much more slowly.

Mixture modelling of high spectral and spatial resolution imaging spectrometer data has been shown to be a useful tool for characterization of the amount and distribution of surface constituents (e.g. Mustard and Pieters, 1987a, Gillespie et al, 1990). In addition, mixture modelling assuming linear mixture systematics has been shown to be a reliable and quantitative method for total analysis of multi- and hyper-spectral data from calibration through to a detailed description and model of the surface (Adams et al, 1986; Smith et al, 1990a). In the present analysis, spectral mixture modelling is applied to AVIRIS data over a field site in the foothills of the Sierra Nevada, California to identify and map the principal surface components. The terrain consists of a heterogeneous mixture of soil, rock, and vegetation in a hilly environment that has many slope changes over short spatial distances. The highly variable illumination conditions and heterogeneity in relative amounts of surface components presents a significant challenge to the effective analysis of imaging spectrometer data.

The primary goal of this investigation is to identify the major surface constituents on the basis of spectral properties and map the distribution and abundance of the constituents. The surface elements mapped will be interpreted to determine which are associated with transient surface components such as vegetation and which are associated with the less transient soil and bedrock properties. As stated above, short term changes in the land surface are likely to be concentrated in transient surface constituents such as vegetation. To quantitatively compare and understand scenes in a multi-temporal context, the transient surface constituents must be decoupled from the less transient elements such as soils. However, soils contain a dynamic mixture of organic and inorganic components, some of which may have a rapid response to land surface changes (e.g. humus). Since soils will play an vital role in global change research, it is important to determine from the standpoint of remote sensing if different soils can be identified as distinct from standing vegetation, are they characterized by specific compliments of organic or inorganic constituents, and

can those constituents be uniquely identified. It will be shown in this analysis that transient surface components green vegetation and senescent grasses are distinct spectrally and the abundances are mapped in a spatial context. Three additional surface components are also mapped. The spatial distributions and abundances are interpreted to indicate that these components are closely related to different soils while the spatial distributions and spectral properties appear to be coupled, to first order, to bedrock composition.

II Field Site

The study area lies primarily within the Kaweah serpentinite melange in the western foothills of the Sierra Nevada near Fresno CA (Figure 1). The topography is hilly, but smoothly varying with few extensive rock faces or cliffs and a maximum topographic variation of ≈200 meters. The bedrock is dominated by the components of a tectonically deformed ophiolite melange in the western half of the site and volcaniclastic sediments and primarily granodiorite plutonic rocks of the Sierra Nevada in the eastern half. The distribution of primary rock types and general mineral constituents of the melange are well known from extensive field studies (Saleeby, 1977; 1978; 1984). In the melange, substantial blocks of the coherent ophiolite components (oceanic basalt, gabbro, peridotite) up to several kilometers long generally occupy the higher topographic regions while the intervening regions are composed of the compositionally complex melange matrix. Compositional variation in the large blocks is low while in the matrix composition varies tremendously on all scales from centimeters to kilometers. The overall composition of the ophiolite melange is mafic to ultramafic with abundant magnesium and iron but little potassium, sodium, and aluminium. The regional extent of the melange can readily be recognized by the distinct lack of trees and uniform cover of soils and grasses on surfaces underlain by melange bedrock. On surfaces underlain by granodiorite, trees are more common, though still sparse.

Rock outcrops are sparse and largely restricted to hilltops and ridges. Hill slopes are covered by a variable mixture of soil and, during the dry season, senescent grasses. Lithic fragments up to a few centimeters in length are common in the soils on the hill slopes. Valley floors are filled with alluvial deposits which can be quite thick along Yokohl Creek. Relict alluvial fans and cones are observed where some of the valleys exit into the larger valley associated with Yokohl Creek. Several small, old, debris flows, now covered by grass, occur along the base of the hills in the north-central part of the field area. There is no evidence of any major active transport of surface materials, which suggests the surface is in a stable erosional state.

Surface Materials

In terms of visible to near-infrared reflectance properties, there are four primary types of surface materials exposed in the field site: green vegetation, senescent grasses, rock, and soil.

The lithologic components underlying the field site are extraordinarily diverse. The matrix of the melange is particularly complex with mineral chemistries and modal abundances varying greatly even at the scale of a few centimeters. Because mafic minerals exhibit strong absorptions at visible to near-infrared wavelengths, these components are well distinguished at AVIRIS wavelengths. A selection of reflectance spectra representative of the diversity of the block and matrix lithologies are shown in Figure 2a. All spectra shown are of exposed, naturally occurring, weathered surfaces. These materials are characterized, and distinguished by the strength, position, and shape of the broad ferric and ferrous absorptions between 0.5 and 1.4 μm and the narrow hydroxyl overtone and combination overtones near 1.4 μm and longwards of 1.8 μm. Based on the characteristics of these spectral features it is possible to identify the mineral species (e.g.. Burns, 1970; Farmer, 1974; Hunt and Salisbury, 1970), the abundance of minerals (e.g.Johnson et al, 1983; Clark and Roush, 1984; Mustard and Pieters, 1987a; 1989), and estimate the chemical composition of the minerals (Sunshine et al, 1990; Mustard, 1992). Shown in Figure 2a are spectra of melange lithologies dominated by serpentine (matrix rock) and the amphibole hornblende (altered gabbro). Both exhibit strong Fe^{2+}-Fe^{3+} charge transfer bands near 0.7 μm and Fe^{2+} electronic transition bands near 0.95 and 1.15 μm. Significant quantities of fine-grained disseminated magnetite in these rocks would act to reduce the albedo and attenuate the spectra contrast. Compared to the spectra of the mafic and ultramafic rocks, the spectrum of granodiorite is featureless in this wavelength region, reflecting the dominantly quartz-feldspar mineralogy of this rock type.

Laboratory reflectance spectra of representative vegetation components are shown in Figure 2b. The spectra of the grasses are the most important for this analysis and will be discussed briefly. The spectrum of senescent grass is characterized by a very steep and smooth rise in reflectance between 0.4 and 0.7 μm with cellulose, lignin, and molecular water absorptions longwards of 1.2 μm (Elvidge, 1988). All components of senescent grasses (i.e., stalks, leaves, seed pods) exhibit broadly similar spectral features but the overall albedo varies with the plant part. The differences between the green vegetation and dry grass spectra in Figure 2b are the same as the differences observed in reflectance spectra of deciduous vegetation through senescence. The spectrum of partially decayed grasses differs from senescent grasses primarily in the shape of the spectrum between 0.3 and 1.3 μm where the decayed grasses exhibit a distinct continuum slope. This is due to the breakdown in the structural components of the vegetation. Fires are not uncommon in this region and a spectrum of burnt grass is included for comparison to the green and senescent vegetation. Vegetation absorption features are absent in this spectrum and it is dominated by the spectral properties of carbon.

Laboratory reflectance spectra of bulk soil specimens collected from the field site are shown in Figure 2c. All soil samples were collected from the top few centimeters of the surface and are therefore representative of the material that will interact with solar radiation and be detected by the

AVIRIS sensor. Soils contain variable combinations of liquid, mineralogic, and organic constituents, all of which contribute to the observed reflectance (c.f. Bowers and Hanks, 1965; Condit, 1972; Stoner and Baumgardner, 1981; Huete and Escadafal, 1991). Common to all these spectra are the bound water and hydroxyl absorptions near 1.4 and 1.9 μm. Molecular water also contributes to the general decrease in reflectance at wavelengths longer than 2.2 μm. Narrow absorptions near 2.2 and 2.3 μm are due to Al-OH and Mg-OH combination overtones in mineralogic soil constituents. In the visible to near-infrared wavelength region (0.3 to 1.7 μm) the spectra of these soils are primarily distinguished by the presence or absence of absorptions associated with Fe^{2+} and Fe^{3+} and by organic carbon absorptions in humus (Huete and Escadafal, 1991). The reddish soil (D) exhibits a strong absorption near 0.5 μm and a weak absorption near 0.9 μm which are typical of charge transfer absorptions and indicates the presence of ferric and ferrous iron. The spectra of soils B and C exhibit weak charge transfer absorptions superimposed on the strong positive continuum slope again pointing to the presence of Fe^{2+} and Fe^{3+}. However the continuum shape of soils B, C, and E, which is characterized by a steady rise in reflectance to a slightly concave shape, can be indicative of absorptions related to organic carbon (Huete and Escadafal, 1991). The subtle inflexions are likely due to Fe^{2+} electronic transition absorptions indicating that the Fe^{2+} is in octahedral coordination, probably in lithic fragments or minerals in the soil.

It is unlikely that such well defined mineral absorptions seen in Figure 2a will be observed in the AVIRIS data. The rock exposures are too small and distributed to contributed significantly to the reflectance spectra measured by AVIRIS and the rock outcrops have variable covers of lichen and mosses that further limit direct exposure. However, the spectra shown in Figure 2a provide some indication of the spectral variability and diversity of bedrock underlying the region which may be detected in the surface spectra. It is anticipated that the primary signal detected by the AVIRIS sensors will be dominated by the spectral properties of soils and senescent grasses. The key questions in this analysis are: can the relative contributions of soils and grasses be determined?, can different soil spectral types be identified?, what is the relationship to the underlying bedrock?, and are there any small absorptions superimposed on the general soil-grass continuum that are diagnostic of bedrock composition.

III Analysis

Data Reduction and Calibration Estimates

AVIRIS data were acquired over this region on October 2, 1989 under generally clear conditions. An image of the surface reflectance at wavelength channel 650 nm is shown in Figure 3. Although it was not possible to coordinate field activities for this overflight, field observations, collection of surface samples, and measurement of field reflectance using the PIDAS spectrometer

(Goetz, 1987) had been accomplished in June and September 1987. There are no time-invariant, compositionally homogeneous regions in the AVIRIS scene that are large enough to be used as calibration targets. However an extensive library of spectra representative of the surface materials in the field site has been developed, and therefore the mixing-method approach to calibration discussed in detail by Smith et al (1990a) and Gillespie et al (1990) was employed as a guide for calibration. The raw AVIRIS data were first corrected to radiance using engineering and calibration files provided by JPL. These corrected data were visually inspected, channel by channel, for data quality and image channels with poor quality were discarded. Data from the D spectrometer (1.84-2.45 μm) were of uniformly low quality and therefore not used in this analysis. A total of 104 out of the 160 channels in spectrometers A, B, and C (0.41-1.86 μm) was selected. Most of the discarded bands occur in the wavelength regions of strong atmospheric water absorption bands near 0.94, 1.13, and 1.4 μm.

In theory, the number of possible endmembers in a spectral mixture analysis is determined by the spatial and spectral resolution, and the dimensionality of the data (i.e. total number of bands). However, in practise, the number of unique endmembers is generally far less than the number of bands in hyperspectral systems. This is because adjacent channels in hyperspectral data are highly correlated, and therefore redundant, and for spatial resolutions measured in the 10's of meters, the spectral variance of a scene is dominated by a small number of common surface constituents (e.g. grass, soil, etc). The spectral properties of the common constituents combine, in different fractional proportion for each pixel, to form a "continuum" that explains most of the spectral variance. This "continuum" differs from conventional continuua, which are smooth maximum limiting curves from which spectra depart in discrete absorptions. Unlike conventional continuua, a mixture "continuum" frequently contains strong absorptions that exist in the spectra of the common constituent endmembers. Unusual or unmodelled components and absorptions that occur in low abundances or have very weak absorptions, can be detected in residual images (difference between spectrum and modelled continuum as a function of wavelength).

A subsection of the total image that included agricultural lands was extracted for initial analysis and estimation of reflectance calibration coefficients. An interactive linear mixture analysis was performed on this subset to identify the image endmembers. The theory and methods employed in this process are discussed in detail by Smith et al (1990a) and Gillespie et al (1990). Image endmembers were initially defined using statistical analysis of spectral variance and a basic understanding of the surface constitutents from field observations. They were then refined by examining intermediate solutions to the mixture model and re-selection of the pixel locations of the image endmembers based on the root mean square (rms) error and fraction images. A solution is considered valid when 1) fraction values across the scene are mostly between 0.0 and 1.0, 2) average rms error for the image is close to that expected for the noise equivalent DN, 3) the image

of rms error contains little structure or spatial information, and 4) the fraction images are spatially coherent and consistent with field observations. Throughout these analyses, a model "shade" endmember is included in addition to the image endmembers. "Shade" is an idealized zero-reflectance endmember that models albedo variations that are due to the effects of variable illumination and shading in the scene, (Adams et al, 1986; Gillespie et al, 1990). For the initial subset of the total scene four image endmembers plus "shade" were required to accurately model the scene radiance.

The uncalibrated spectra of the four AVIRIS image endmembers were then transformed from radiance values to the reflectances of the spectral library developed for this site using the linear gain, offset, and fractional abundance relationships given by Smith et al (1990a) and Gillespie et al (1990). The purpose of this procedure was to derive a set of calibration coefficients to correct for the additive and multiplicative effects of instrument and atmosphere and thereby convert the AVIRIS radiance to an estimate of surface reflectance. Convergence to an acceptable solution was hindered by the low spectral contrast between the image endmembers and the lack of relevant spectra of green vegetation in the spectral library used. Although the general shapes of spectra of green vegetation are very similar, the strength of the red edge absorption is variable among species and does not scale linearly. Since green vegetation has the greatest spectral contrast in this AVIRIS scene, an improper green vegetation spectral endmember can adversely effect the gain and offset values determined. However, inspection of the gain and offset factors indicated only small variations among the solutions for the offset term. Since the additive terms are more critical than the multiplicative terms for mathematical analyses of spectra (e.g. band or spectral ratios), an average of the offset terms from several solutions was subtracted from the AVIRIS radiance. To convert to reflectance, a region with an apparently homogeneous cover of dry grass was used as a relative reflectance calibration standard (Mustard and Pieters, 1987b). The library spectrum for the dry grass was acquired with the PIDAS spectrometer from the field area. A plot of the multiplicative and additive terms used to convert the AVIRIS radiance to approximate reflectance is shown in Figure 4. Note that the additive term shows a decrease with increasing wavelength, typical of atmospheric scattering.

Spatial Distributions

In the initial linear mixing analysis of the raw data to derive calibration coefficients, a subset of the total AVIRIS scene was used to expedite the analysis and the evaluation of the calibration. Using the data corrected for estimates of the additive and multiplicative calibration factors (calibrated data) this analysis was expanded to encompass the entire image. All calculations were carried out using the full dynamic range of the AVIRIS data. Interactive spectral mixture analysis of the entire image was performed using successive solutions to refine the number of endmembers

and the physical location from which the spectra of the image endmembers were derived. A total of 5 image endmembers ("dry grass", "green vegetation", "Soil1", "Soil2", "Soil3") plus a model "shade" of 0.01% reflectance (to model illumination effects (Adams et al, 1986)), were required to satisfy the criteria for a valid solution discussed above. The physical locations from where these endmembers were extracted are shown in Figure 3. Additional endmembers cause the solutions to violate criteria 1 and 4 while fewer endmembers violate criteria 2 and 3. The average rms error for the entire image is less than 3% reflectance. Inspection of the rms error image shows a high quality fit with only a few regions of high error, generally associated with green vegetation components such as irrigated lawns and along water courses. The strength of the chlorophyll absorption to near-infrared reflectance, and compliment of "shade", leaves, and woody material for these areas differ from the image endmember for green vegetation which was taken from an orchard. The fraction images showing the spatial distribution and abundance of the five image endmembers plus "shade" are are shown in Figure 5.

The fraction images provide a framework for exploring the many interesting relationships amongst soil, rock, and grass in this area. Note that the fraction images are largely uncorrelated with illumination (compare to the complimented "shade" image). This indicates that primarily the fractional contributions to each AVIRIS spectrum from the image spectral endmembers are being identified, and not effects of illumination. The elements of green vegetation are extremely well modelled and partitioned into the vegetation fraction image. This is expected since green vegetation exhibits the most spectral contrast of all the endmembers. Throughout most of the field area, and especially in regions underlain by the mafic and ultramafic lithologies of the Kaweah ophiolite melange, green vegetation is essentially absent and is localized in irrigated fields and along water courses. In the northwestern portion of the image area, however, slightly elevated values for green vegetation are observed and appear as discrete points. This region is associated with the more silicic substrate of the Cretaceous batholiths. The discrete points correspond to individual trees. The grass endmember is highly correlated with the albedo (though not illumination) as seen in Figure 3. The spatial patterns agree with general field observations made in 1987, but there have been some changes in the distribution of dry grass inferred from visual examination of airphotos, SPOT, and thematic mapper data. The correlation of changing patterns with field boundaries suggests that shifts in the principal sites of herbivore grazing are an important cause of the observed variations. Fires have also affected small areas (e.g., north central part of image area, indicated by the white arrow in Figure 3).

The other three fraction images in Figure 5 are interpreted to represent different primary surface units consisting of surface soil and partially decayed vegetation, principally grass. As such they do not uniquely identify a specific soil type, but nevertheless display spatial patterns that can be interpreted according to the known distributions of lithologic substrates (Compare to Figure

1b). These endmembers are referred to as "soils" in the following discussion for convenience. The distribution of "Soil1" is concentrated in the eastern half of the image area. The highest fractions are found in the alluvial deposits along the southern border of the river valley, and in the exposures of Cretaceous granodiorite in the northeastern and south-central parts of the image. Within the area underlain by volcaniclastic sediments, slate, and argillite, the fractions are also uniformly high, though not as high as for the areas mentioned above, and exhibit no evidence of geomorphic control on location or abundance. In the western half of the image the distributions are patchy and discontinuous. Detailed maps of the block types and distributions in the melange by Saleeby (1978) indicate a substantial concentration of bedded chert, chert blocks, and chert interbedded with basalt in the portion of the image slightly north and west of the center (indicated in Figure 1b). A relatively large zone of moderate "Soil1" concentration is found in this same region. High abundances values of "Soil1" are observed to cross from the regions of low green vegetation abundance in the northeast to a region of no green vegetation in the south, and show no obvious correlation with anthropogenic effects. Therefore "Soil1" shows higher overall abundances in regions underlain by granodiorite, volcaniclastic, and chert relative to regions underlain by melange lithologies. The correlation of the observed distributions and abundances of "Soil1" with general bedrock composition and not at all with vegetation or anthropogenic activity argue that the spectral properties of "Soil1" are strongly controlled by substrate composition.

The distribution patterns observed for "Soil2" are broadly complimentary to "Soil1" in that "Soil2" is widely distributed but concentrated in the western half of the image. In the eastern part of the image, this spectral unit is localized along just a couple of valley bottoms and also along the flood plain of the creek. Upon closer examination, "Soil2" exhibits the highest abundances locally on the lower slopes of the hills and more extensively in the broad valleys of the north and south. In this manner, the distribution pattern of "Soil2" differs from "Soil1". "Soil1" is broadly distributed with few obvious concentrations related to the general surface morphology while "Soil2" is apparently concentrated on the lower slopes and valley bottoms. The distribution patterns in the western region correspond extremely well with the general lithologic boundaries of the mafic-ultramafic melange substrate. This implies that at least for some of the region, the spectral properties of the surface soil reflects the composition of the underlying bedrock. The combined abundances of "Soil1", "Soil2", and dry grass account for the majority of the surface spectral properties of the non-vegetated regions in this image.

"Soil3" is concentrated along valley floors in the northwestern region, and can be detected in many small narrow valleys connecting to the main valleys. This imparts a filamentous or web-like appearance to the fraction image for this endmember. Like "Soil2", "Soil3" displays low to absent abundances in the terrain underlain by volcaniclastic sediments in the south eastern portion of the image. But unlike "Soil2", it does appear in modest abundances in conjunction with "Soil1" in the

north eastern part of the image. Finally, "Soil3" exhibits a very interesting, discontinuous but spatially coherent zone of elevated abundances that forms an arcuate belt extending from the central part of the image towards the southeast and around the edge of the Cretaceous granodiorite outcropping along the southern image border. This belt correlates extremely well with a series of faults extending around the plutonic plug, through the volcaniclastic sediments, and into the melange where the identification of the faults is lost in the complexly deformed and compositionally complex melange matrix. The association of the spectrally distinct region with fault traces and a pluton strongly suggests a genetic link. It is postulated that the intrusion served as a heat source that established hydrothermal circulation that lead to hydrothermal alteration of rocks along the faulted areas.

The overall distribution patterns associated with "Soil3" imply a range of compositional controls on the spectral properties. The valley floor concentrations may reflect a special environment for soil formation or, because the valleys are easily accessible and travelled, a surface that is more disturbed by human and animal activity. Field observations would support the latter explanation, since footpaths, animal trails, and jeep trails are very common along all the valley floors. "Soil3" compliments and co-varies with both "Soil1" and "Soil2", indicating that substrate composition alone does not define the spectral properties of this endmember. However, the absence of "Soil3" in the region underlain by volcaniclastic sediments, and the arcuate zone of enhanced abundances cutting through this region, imply that lithologic substrate must have some effect on the surface spectral properties.

This analysis of endmember fraction images and observed correlations to the general geologic features in Figure 1b indicate that the spectral properties of the three "soil" endmembers are at least partially controlled by bedrock composition. The other endmembers, green vegetation, grass, and "shade", are more strongly controlled by agricultural cultivation, land use, and topographic shading (for "shade"). Spectral mixture analysis has therefore permitted the mapping of the primary surface spectral units and the identification of surface spectral units more strongly associated with soil and substrate composition. Because the spectral effects of vegetation and shading have been largely isolated, a detailed examination of the compositional character and variations of the soil properties is possible. This can be summarized by presenting the three soil fraction images in a three color representation with "Soil1" as blue, "Soil2" as red, and "Soil3" as green. To display the relationships between compositional variation and morphology better, the soil fraction images have been divided by the "shade" fraction image, which essentially superimposes the spatial variations in the soil abundances on a shaded relief representation of the topography. This is shown in Color Plate 1. This highlights the contrast between the uniform spectral, and interpreted compositional, properties of the surfaces underlain by the volcaniclastic and granodiorite lithologies vs the complex variations associated with surfaces underlain by the

mafic-ultramafic melange. The arcuate zone cutting across the volcaniclastic substrate and extending around the granodiorite outcrop in the south central part of the image that correlates with inferred faults in the substrate (Saleeby, 1979) is very clearly defined. Although the inferred faults are in rocks of similar bulk composition and lithology, the spectral properties are obviously distinct.

Interpretation of Image Endmember Spectral Properties

AVIRIS approximate reflectance spectra of the five image endmembers used to compute the distribution and abundance of surface components are shown in Figure 6. These spectra are averages of about 20 spectra each and the image locations from where the spectra were taken are shown in Figure 3. The spectrum of dry grass exhibits the characteristic steep rise in reflectance and smoothly varying spectrum discussed above in the section on surface components. The green vegetation spectrum exhibits classic features of green vegetation including the small 0.55 μm reflectance peak, the sharp edge of the chlorophyll absorption near 0.7 μm, and leaf water absorptions near 1.0, 1.3, and longwards of 1.5 μm. The spectra of these endmembers are distinct and exhibit strong spectral contrast relative to the other endmembers. This is reflected in the fraction images, which are sharp and apparently free of noise, indicating that these endmembers are independent and represent distinct surface components.

The soil spectra are distinguished primarily by the spectral shape between 0.5 and 1.3 μm, the magnitude of the drop in reflectance from 1.32 to 1.50 μm, and the spectral shape between 1.5 and 1.7 μm. The spectrum of "Soil1" clearly exhibits some characteristics of the dry grass spectrum. Although there is a relatively steep continuum slope from 0.6 to 1.3 μm, there is a large drop in the intensity across the data gap near 1.4 μm and there is the typical dry grass shape between 1.5 and 1.7 μm. Since the process of decay can impart a steep continuum slope to a grass spectrum (Figure 2b), this drop in intensity and shape provide the best indicators for the presence of grass components on the surface. However, analysis of the fraction image for this endmember implies at least a partial control on the spectral properties by the soil properties and substrate. Therefore the spectrum of this endmember is interpreted to contain the surface components of partially decayed grass and soil developed over volcaniclastic and granodiorite substrate.

The endmember spectra of "Soil2" and "Soil3" differ qualitatively from "Soil1" in the continuum properties and spectral shape at wavelength channels longer than 1.3 μm. As shown in Figure 6, both exhibit an apparently flatter continuum slope, with two distinct breaks in slope near 0.6 and 0.7 μm. Also they both show a less intense drop across the data gap at 1.4 μm , and the spectral shapes between 1.5 and 1.7 μm are somewhat more featureless than "Soil1", and much more featureless than the dry grass and green vegetation. To emphasize the relative differences between the endmember soil spectra and de-emphasize possible calibration difficulties in the

interpretation of these data, the ratio of soils 2 and 3 to "Soil1" is computed and shown in Figure 7. This indicates that "Soil2" relative to "Soil1" has a less steep continuum slope from 0.5 to 1.0 μm (decreasing ratio), but similar continuum properties from 1.0 to 1.7 μm (constant ratio). "Soil3" relative to "Soil1" exhibits a less steep, relative continuum between 0.5 and 0.9 μm but "Soil3" displays a significantly greater continuum slope than "Soil1" (increasing ratio) in the wavelength region 0.90 to 1.7 μm. In summary, both "Soil2" and "Soil3" differ from "Soil1" with less steep continuum slopes between 0.5 and 0.9 μm. "Soil2" then parallels the general spectral properties of "Soil1" between 0.9 and 1.7 μm while "Soil3" shows an increase in spectral continuum.

There are two major possibilities for the observed differences in the spectral properties of the soil endmembers: mineralogic and organic. If the differences are due to mineralogic factors, comparison of the soil endmember spectral properties to the laboratory spectra of the primary surface components shown in Figure 2 suggests that Fe^{2+} and Fe^{3+} absorptions could be contributing to the spectral properties of "Soil2" and "Soil3". It is observed that both rock and soil spectra from the melange exhibit a break in slope around 0.6 μm where Fe^{2+}-Fe^{3+} charge-transfer absorptions begin to become prominent. Between 0.6 and 1.8 μm, some soils (A,D, and E) show featureless spectra that have progressively less steep continuum slopes. Other soils (B, C) show evidence of Fe^{2+} and Fe^{3+} absorptions, as well as a strong and, in some cases, increasing continuum slope out to approximately 1.8 μm. The spectra of the melange rocks show strong Fe^{2+} and Fe^{3+} absorption between 0.6 and 1.1 μm, and a prominent increase in spectral continuum slope from 1.1 to 1.8 μm. In soils developed over the mafic and ultramafic bedrock in the melange, the combination of Fe^{2+} and Fe^{3+} absorptions could cause observed differences from the spectral properties of "Soil1" shown in Figure 7. Organic matter can impart a similar overall absorption between 0.6 and 1.2 μm (Stoner and Baumgardner, 1981; Condit, 1972; Huete and Escadafal, 1991) that is similar to some of the curve shapes for the soil spectra. However, organic constituents would also contribute to the drop in reflectance between 1.35 and 1.5 μm. Therefore, it is apparent that "Soil1" is likely to contain the most organic component relative to endmember soils 2 and 3, and the distinctions of "Soil2" and "Soil3" from "Soil1" is primarily mineralogic.

IV Conclusions

The field site investigated presented significant challenges to the quantitative use of remote-sensing data. Although not mountainous, the topography is very hilly and the illumination geometry varies substantially on very short spatial scales. The surface is covered by a heterogeneous mixture of green vegetation, dry and decaying grasses, and soils. The more level areas are cultivated and much of this cultivation is in the form of irrigated fields and orchards. In the hilly terrain, the land is used principally to graze cattle and horses and the grazing patterns

change frequently. Also, range fires are not uncommon. Finally, the bedrock geology is extremely complex, varying from a relatively homogeneous substrate in regions underlain by Cretaceous granodiorite to the highly variable mafic to ultramafic Kaweah melange, in which the composition can vary quite substantially on the scale of a few meters. In order to derive a realistic model or quantitative description for this complex surface, one must isolate transient surface components such as the amount of green vegetation, dry grass, and illumination, from the less transient surface elements such as soils and bedrock.

The high spectral and spatial resolution reflectance data provided by AVIRIS provides an extraordinary wealth of information about surfaces. However, in a terrain such as this, the information is not always evident. Distinct and well defined absorptions diagnostic of the composition of surface constituents are largely absent in the AVIRIS data, except from materials like green vegetation which have a high spectral contrast. Instead, the reflectance properties of all the surface constituents are mixed such that the spectral contrast in any given pixel is muted and unique identification of surface constituents is challenging. Also, as the relative proportions of components vary through time due to changing land use, and to the effects of short- and long- term climatic fluctuations, these changes may be misinterpreted using traditional classification and change detection techniques.

In this study, spectral mixture analysis was used to identify and map the distribution and abundance of five primary surface components and also to model the effects of variable illumination. This approach successfully separated the transient surface spectral components of illumination, dry grass, and green vegetation, from the more stable surface spectral components associated primarily with soils. Although the "soils" mapped in the approach taken here will by nature contain transient elements (primarily as varying proportions of organic constituents), the correlation between the soil fraction images and bedrock geology indicates a lithologic influence on the soil spectral properties, and therefore composition. A more sophisticated application of spectral mixture analysis as described by Smith et al (1990a; 1990b) in which the data are deconvolved into fraction images of well characterized spectral endmembers from a library, would better characterize soil compositions and abundances. Nevertheless, the distinction between these soil image endmembers in a spectral context is very subtle, yet the spatial distributions observed in the fractions images reveal coherent and interpretable patterns. This therefore demonstrates the tremendous value of high spectral and spatial resolution data in discriminating subtle differences in soil composition, despite the complicating effects of highly variable transient surface components.

Acknowledgements: Support from NASA grant NAGW-1118 is gratefully acknowledged. Many thanks to Rob Green for assistance in operating the PIDAS instrument and collecting data in the field, J. Saleeby for discussions of the geology and providing detailed field maps, C. Pieters

for thoughtful collaborations and discussions in and out of the field, and to J. Adams, M. Smith, and S. Willis for their contributions to my understanding of the linear mixing approach. Careful reviews by A. Gillespie and an anonymous reviewer are also acknowledged.

References

Adams, J. B., Smith, M. O., and Johnson, P. E. (1986), Spectral mixture modeling: A new analysis of rock and soil types at Viking Lander 1, *J. Geophys. Res.* 91:8113-8125.

Bowers, S. A., and Hanks, R. J. (1965), Reflection of radiant energy from soils, *Soil Sci.* 100:130-138.

Burns, R. G. (1970), *Mineralogical Application to Crystal Field Theory*, Cambridge University Press, London. 224 pp.

Clark, R. N. and Roush T. L. (1984), Reflectance spectroscopy: Quantitative analysis techniques for remote sensing applications, *J. Geophys. Res.* 89:6329-6340.

Committee on Earth Sciences (1990), Our Changing Planet: The FY 1991 U.S. Global Change Research Program, 60 pp.

Condit, H. R. (1972), Application of characteristic vector analysis to the spectral energy distribution of daylight and the spectral reflectance of American soils, *Appl. Opt.* 11:74-86.

Elvidge, C. D. (1988), Vegetation reflectance features in AVIRIS data, *Int'l Symposium Rem. Sens. Envir., Sixth Thematic Conference on Remote Sensing for Exploration Geology*, 169-182.

Farmer, V. C. (1974), *The Infrared Spectra of Minerals,* The Mineralogical Society, London, pp. 539.

Gillespie, A. R., Smith, M. O., Adams, J. B., Willis, S. C., Fischer, A. F. III, and Sabol, D. E. (1990), Interpretation of residual images: Spectral mixture analysis of AVIRIS images, Owens Valley, California, In *Proc. of the Second Airborne Visible/Infrared Imaging Spectrometer (AVIRIS) Workshop* (R. O. Green, Ed.) JPL publication 90-54:243-270.

Goetz, A. F. H. (1987) The portable instant display and analysis spectrometer (PIDAS), In *Proc. of the Third Airborne Imaging Spectrometer Workshop* (G. Vane, Ed.) JPL publication 87-30:8-17

Huete, A. R. and Escadafal, A (1991), Assessment of biophysical soil properties through spectral decomposition techniques, *Remote Sens. Environ.*, 35:149-159.

Hunt, G. R. and Salisbury J. W. (1970), Visible and near-infrared spectra of minerals and rocks: I Silicate minerals, *Mod. Geol.* 1:283-300.

Johnson, P. E., Smith, M. O., Taylor-George, S., and Adams, J. B. (1983), A semi-empirical method for analysis of the reflectance spectra of binary mineral mixtures, *J. Geophys. Res.* 88:3557-3561.

Mustard, J. F., and Pieters C. M. (1987a), Quantitative abundance estimates from bidirectional reflectance measurements, In *Proc. Lunar Planet. Sci. Conf. 17th, Part 2, J. Geophys. Res.* 92:E617-E626.

Mustard, J. F., and Pieters, C. M. (1987b), Abundance and distribution of ultramafic microbreccia in Moses Rock Dike: Quantitative application of mapping spectrometer data, *J. Geophys. Res.* 92:10376-10390.

Mustard, J. F., and Pieters, C. M. (1989), Photometric phase functions of common geologic minerals and applications to quantitative analysis of mineral mixture reflectance spectra, *J. Geophys. Res.* 94:13,619- 13634.

Mustard, J. F. (1992), Chemical composition of actinolite from reflectance spectra (*in press*) *American Mineralogist.*

Roberts, D. A., Smith, M. O., Adams, J. B., Sabol, D. E., Gillespie, A. R., and Willis, S. C. (1990), Isolating woody plant material and senescent vegetation from green vegetation in AVIRIS data, In *Proc. of the Second Airborne Visible/Infrared Imaging Spectrometer (AVIRIS) Workshop* (R. O. Green, Ed.), JPL publication 90-54:42-57.

Saleeby, J. B. (1977), Fracture zone tectonics, continental margin fragmentation, and emplacement of the Kings-Kaweah ophiolite belt,southwestern Sierra Nevada, California, In *North American Ophiolites* (R. G. Coleman and W. P. Irwin, Eds.), Oregon Dept. Geol. Min. Ind. Bull. 91:141-160.

Saleeby, J. B. (1978), Kaweah serpentinite melange, southwest Sierra Nevada foothills, California, *Geol. Soc. Am. Bull.* 90:24-46.

Saleeby, J. B. (1984), Tectonic significance of serpentinite mobility and ophiolite melange, In *Melanges; Their nature, Origin, and Significance*, (L. A. Raymond, Ed.), Geol. Soc. Am. Special Paper 198:153-168.

Smith, M. O, Ustin S. L., Adams J. B., and Gillespie A. R. (1990a), Vegetation in deserts: I A regional measure of abundance from multispectral images, *Remote Sens. Environ.*, 31:1-26, .

Smith, M. O, Ustin S. L., Adams J. B., and Gillespie A. R. (1990b), Vegetation in deserts: II Environmental influences on regional abundance, *Remote Sens. Environ.*, 31:1-26.

Stoner, E. R., and Baumgardner, M. F. (1981), Characteristic variations in reflectance of surface soils, *Soil. Sci. Soc. Am. J.* 45:1161-1165.

Sunshine, J. M., Pieters, C. M., and Pratt, S. F. (1990), Deconvolution of mineral absorption bands: An improved approach, *J. Geophys. Res.*, 95:10169-10175.

Figure Captions

Figure 1. Location and generalized geologic maps summarized after Saleeby (1978). The ground coverage of the AVIRIS window used in this investigation is shown in (a). A more detailed view of the general geology of this window with fault traces indicated is shown in (b).

Figure 2. Representative laboratory reflectance spectra of the major lithologic, vegetation, and soil types from the field site. All spectra were measured in RELAB at Brown University. The horizontal lines near the top of each plot indicates the wavelength coverage of AVIRIS data used in this analysis. Complete visible to near-infrared reflectance spectra are shown for completeness. In (a), the rock spectra are labelled to indicate the primary mineralogy or lithology represented where Serp refers to serpentine, Amphib refers to the amphibole hornblende, and Grano refers to granodiorite. In (b), A is senescent or dry grass, B is partially decayed grass, C is green vegetation, and D is burnt grass. The spectra of the various soils in (c) are discussed in the text. Note the differences in continuum slope caused by differences in the prominence of Fe^{2+} and Fe^{3+} absorptions.

Figure 3. AVIRIS image at wavelength channel 0.655 μm of the area outlined in Figure 1a. North is towards the top of the image. The white arrow points to a region that has recently burned. The labeled boxes show the locations from where the image endmembers were selected for the mixing analysis. Box a is for the green vegetation endmember, box b is the "grass" endmember, box c is the endmember "Soil1", box d is "Soil2", and box e is "Soil3". The "shade" endmember is idealized as spectrally neutral with a reflectance of 1% across all wavelengths. The fraction images for each of these endmembers are shown in Figure 5.

Figure 4. Gain and offset terms used to calibrate the AVIRIS radiance data to reflectance. Offset terms were derived using a linear mixing approach (e.g. Gillespie et al, 1990) and gain values were determined by a relative reflectance methods after removal of the offset terms (Mustard and Pieters, 1987a).

Figure 5. Fraction images for the image endmembers shown in Figure 6. The intensity or brightness corresponds to the fractional abundance of the image endmember where high brightness means greater fractional abundance except for the "shade" endmember, in the upper left hand corner: this fraction image has had a compliment stretch applied to emphasize that the "shade" endmember models surface illumination effects. Bright grey values correspond to 100% and dark grey values to 0%. The sum of all the fraction images is equal to 100%. From the lower right to the upper left, these images

correspond to green vegetation (lower right), dry grass (lower left), "Soil1" (middle right), "Soil2" (middle left), "Soil3" (upper right) and "shade" (upper left).

Figure 6. AVIRIS reflectance spectra of the image endmembers used to model the surface reflectance and calculated the fraction images shown in Figure 5. They are labelled along the right vertical axis and discussed in detail in the text.

Figure 7. The ratio spectra of the reflectances of "Soil2" and "Soil3" divided by "Soil1". These spectra have been normalized to a value of 1.0 at the wavelength 0.55 μm to emphasize relative differences in spectral shape independent of absolute differences in albedo.

Color Plate 1. Three-color image combining the fraction images for the three soil endmembers with "Soil1" in the blue, "Soil3" in the green, and "Soil2" in the red. The fraction images in Figure 5 were used, but have been divided by the fraction image for "shade" to illustrate the soil distributions relative to topography.

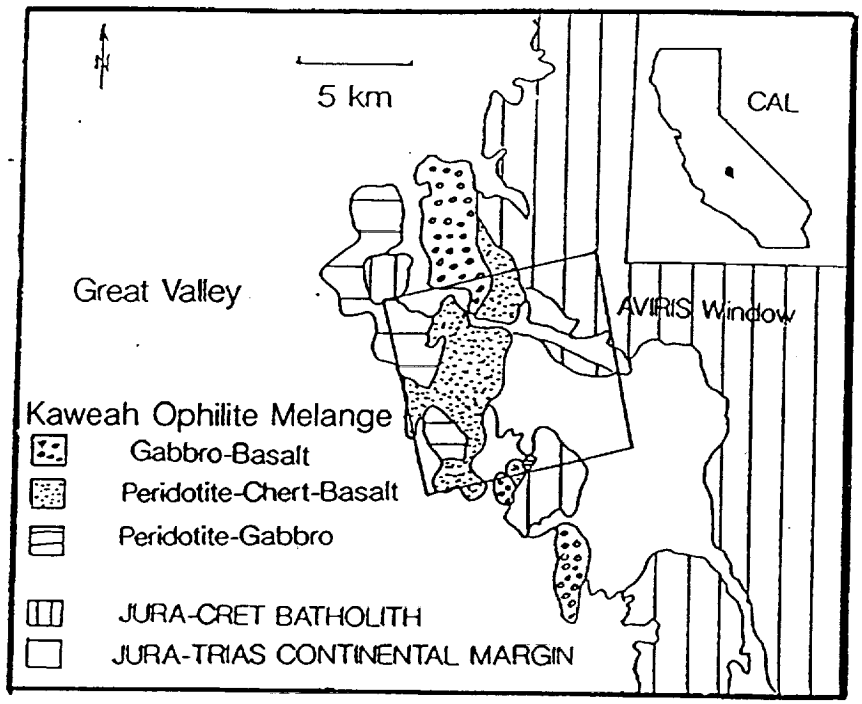
5 km
CAL
Great Valley
AVIRIS Window
Kaweah Ophilite Melange
Gabbro-Basalt
Peridotite-Chert-Basalt
Peridotite-Gabbro
JURA-CRET BATHOLITH
JURA-TRIAS CONTINENTAL MARGIN

a

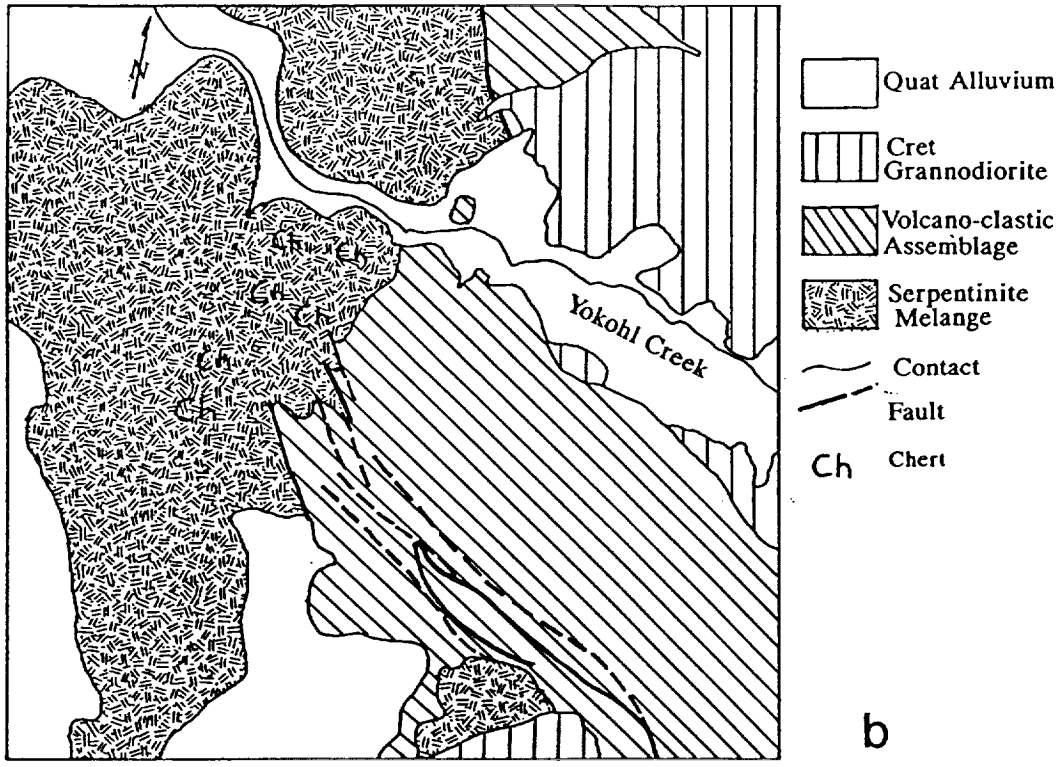
Yokohl Creek
Quat Alluvium
Cret Grannodiorite
Volcano-clastic Assemblage
Serpentinite Melange
Contact
Fault
Ch
Chert

b

Figure 1

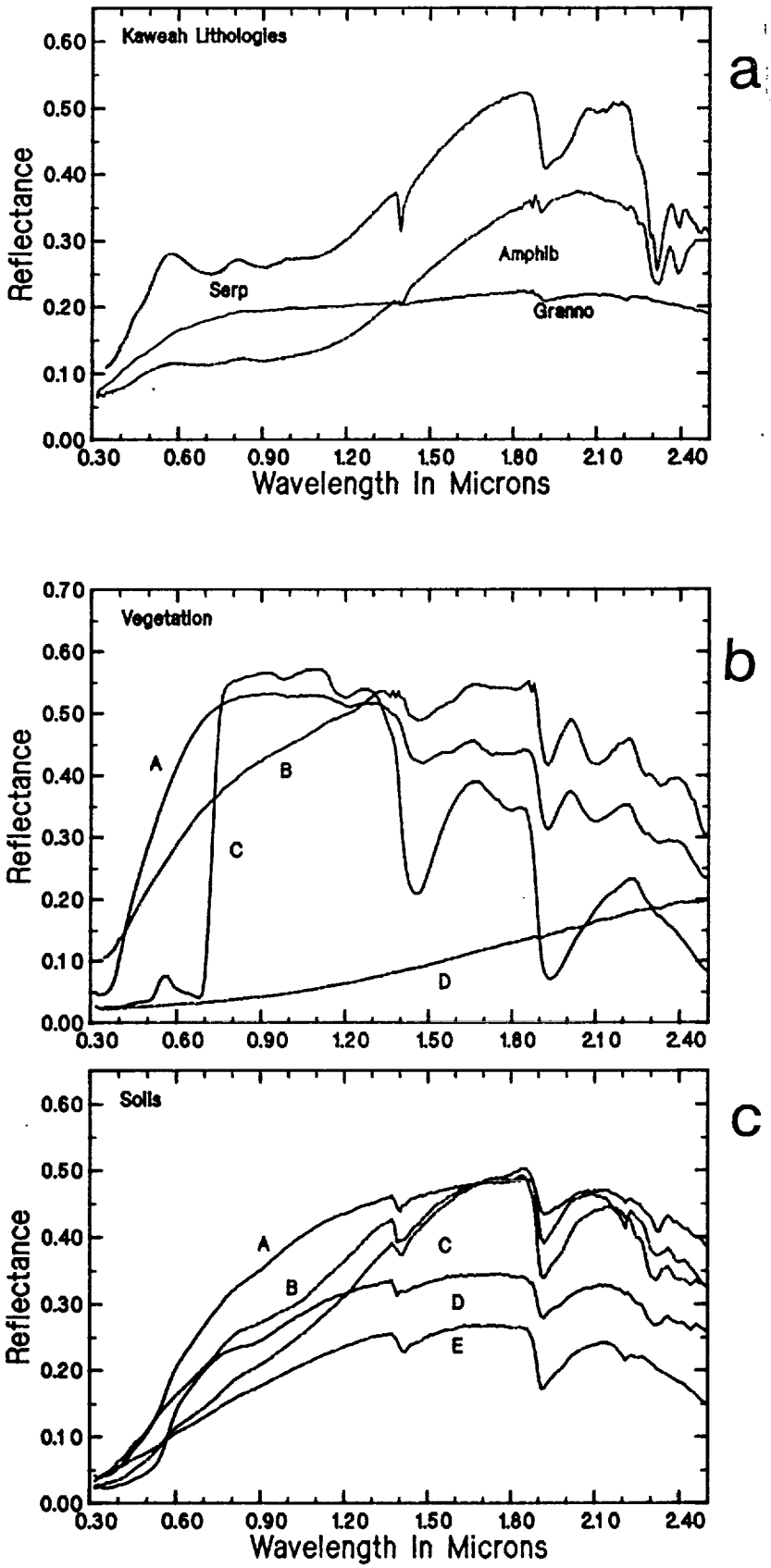
Kaweah Lithologies
a
Reflectance
0.60
0.50
0.40
0.30
0.20
0.10
0.00
Serp
Amphib
Granno
0.30
0.60
0.90
1.20
1.50
1.80
2.10
2.40
Wavelength In Microns
Vegetation
b
0.70
A
B
C
D
Soils
c
E

Figure 2

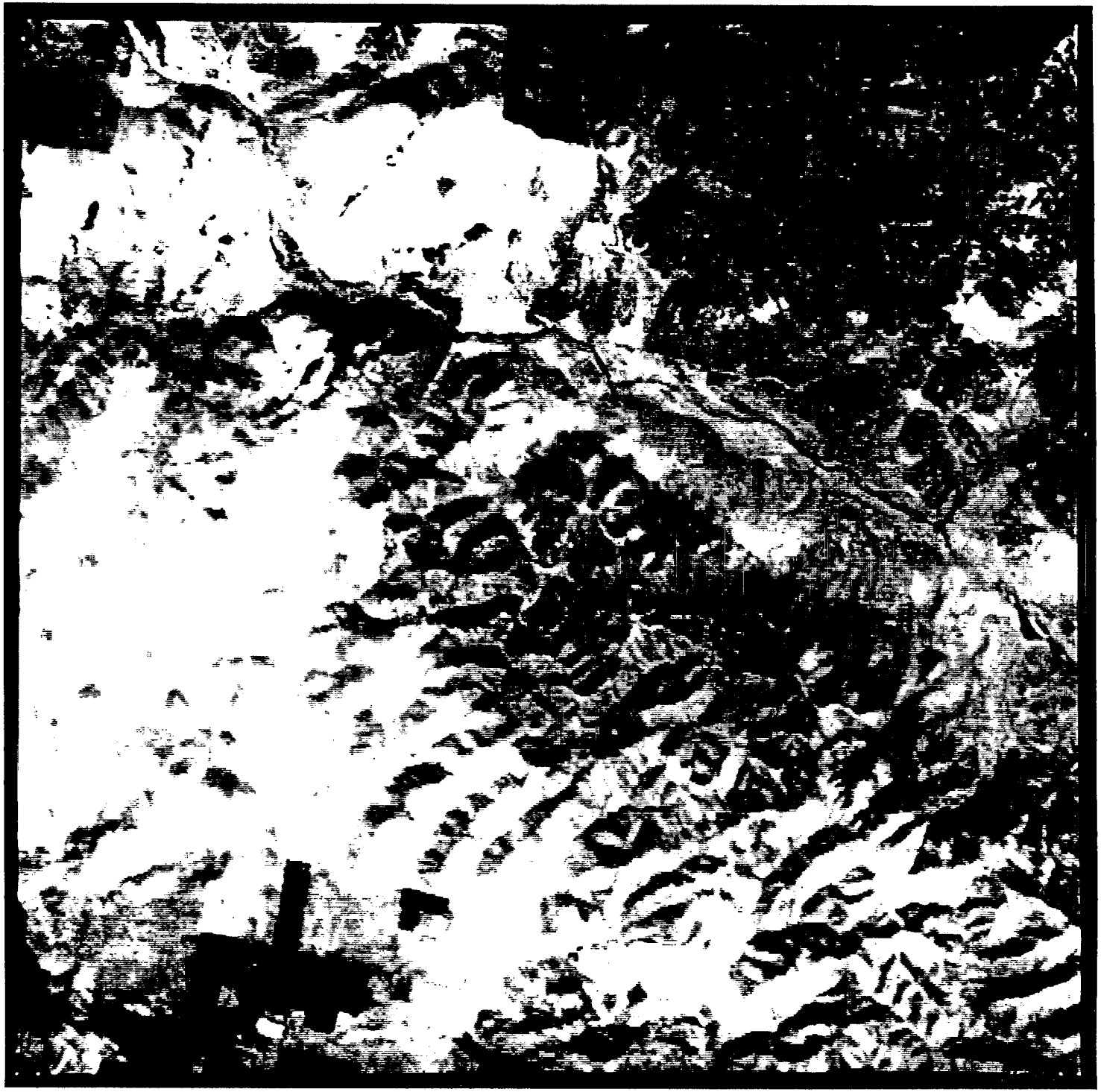

Figure 3

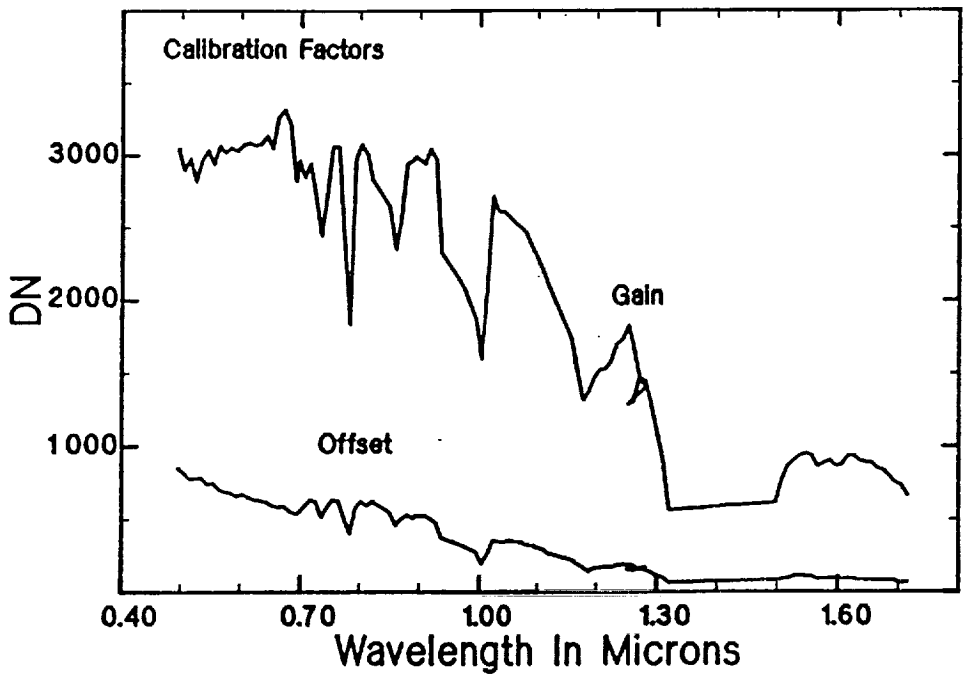
Calibration Factors
3000
2000
1000
DN
Gain
Offset
0.40
0.70
1.00
1.30
1.60
Wavelength In Microns

Figure 4

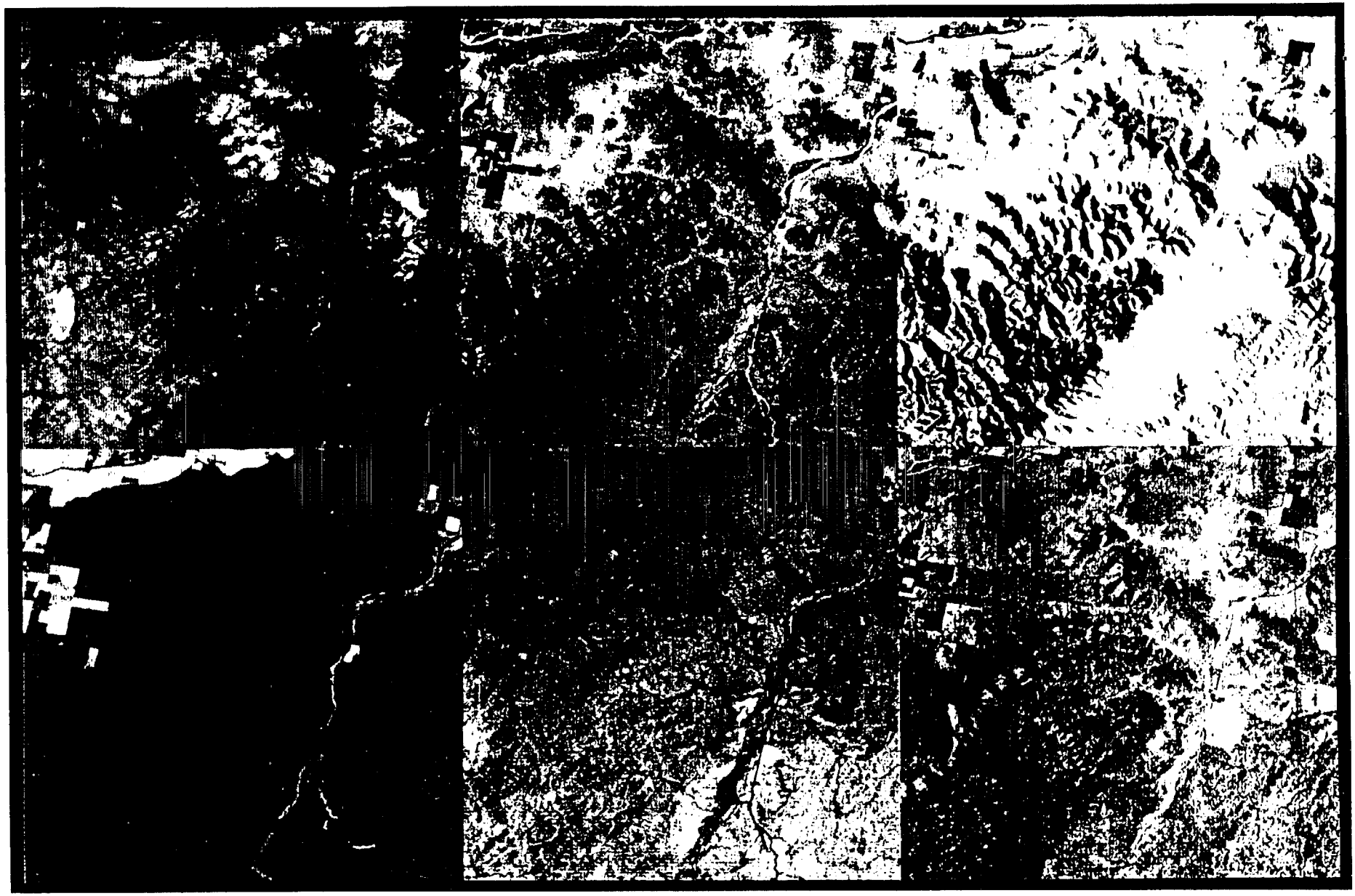

Figure 5

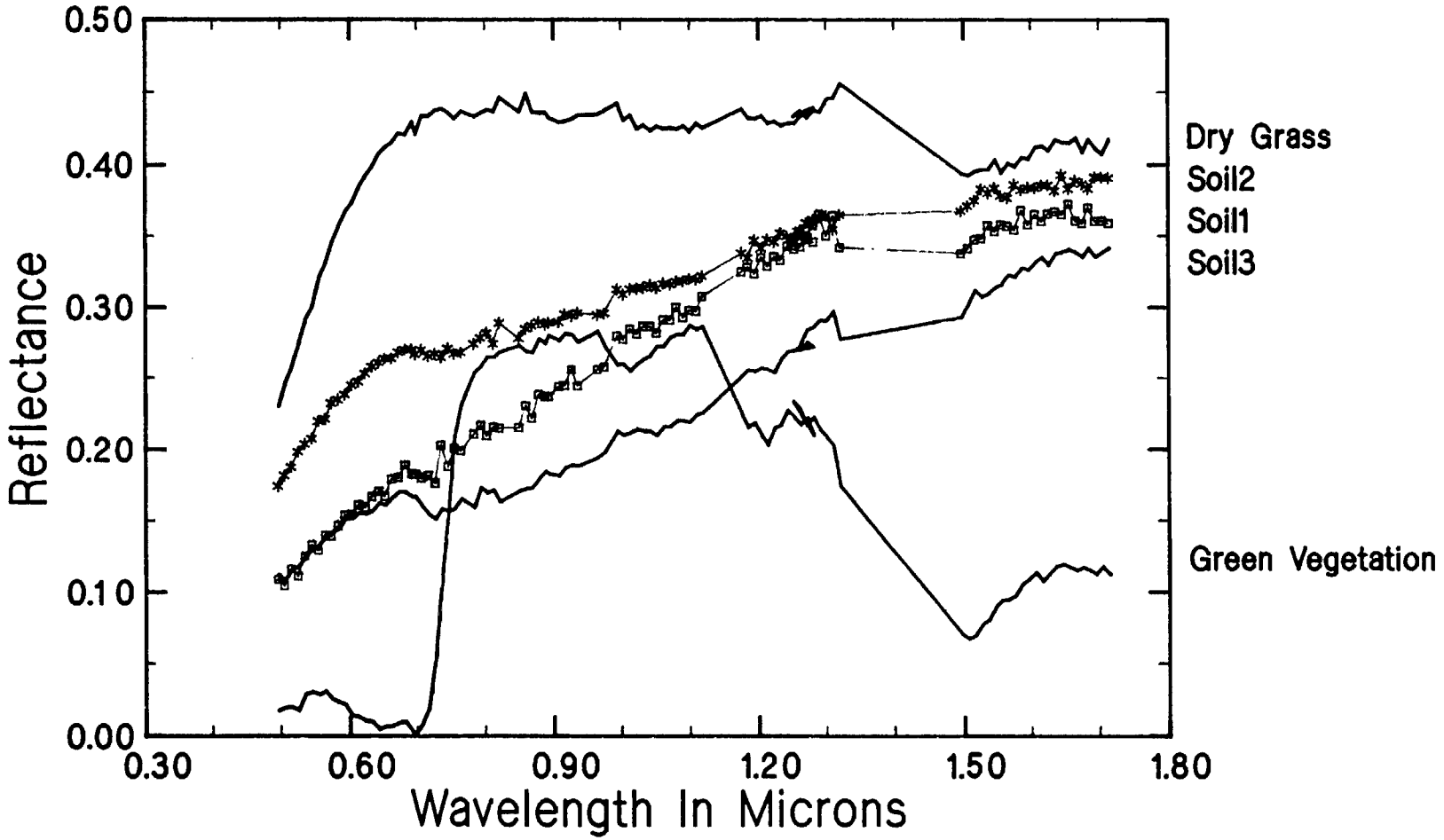
0.50
0.40
0.30
0.20
0.10
0.00
Reflectance
0.30
0.60
0.90
1.20
1.50
1.80
Wavelength In Microns
Dry Grass
Soil2
Soil1
Soil3
Green Vegetation

Figure 6

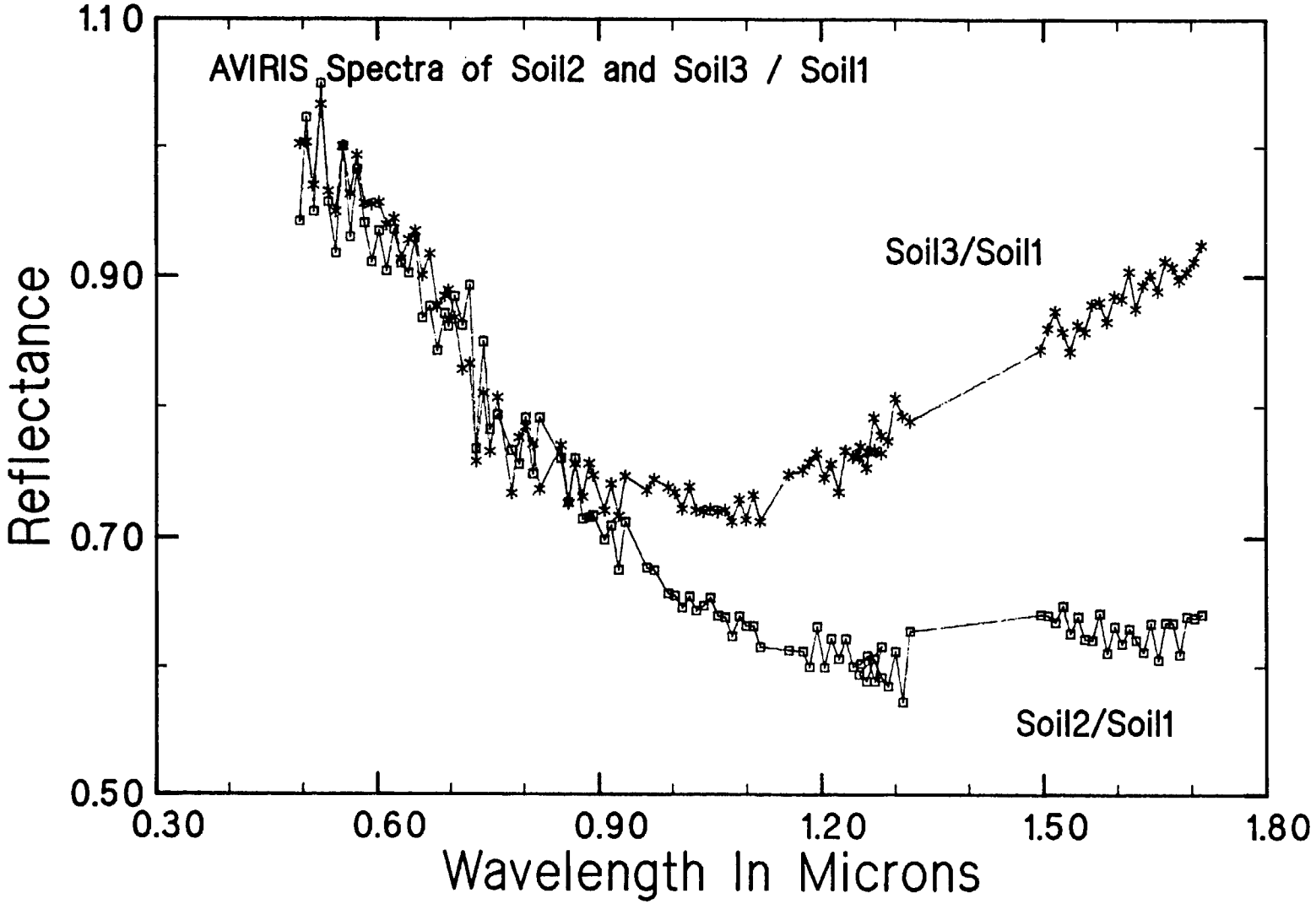
AVIRIS Spectra of Soil2 and Soil3 / Soil1
Soil3/Soil1
Soil2/Soil1
Reflectance
1.10
0.90
0.70
0.50
0.30
0.60
0.90
1.20
1.50
1.80
Wavelength In Microns

Figure 7